Supporting Information for

Oxygen-Carrying Nanoplatform to Reprogram Tumor Immunosuppressive Microenvironment and Enhance Photothermal-Immunotherapy

Ju Huang[a, 1], Xiaojing Leng[a, 1], Tao Jiang[b], Lihong Xu[c], Jun Zheng[a], Mingxiao Fang[a], Jingxue Wang[a], Zhigang Wang[a*], Liang Zhang[a, d*]

[a] *State Key Laboratory of Ultrasound in Medicine and Engineering, Chongqing Key Laboratory of Ultrasound Molecular Imaging, Department of Ultrasound, The Second Affiliated Hospital of Chongqing Medical University, Chongqing 400010, P. R. China*

[b] *Department of Anesthesia, The Affiliated Hospital of Southwest Medical University, Luzhou 646000, P. R. China*

[c] *Institute of Life Sciences, Chongqing Medical University, Chongqing 400016, P. R. China*

[d] *Department of Ultrasound, The First Affiliated Hospital of Chongqing Medical University, Chongqing 400042, P. R. China*

[1] These authors contribute equally to this work.

* Corresponding author. zhigangwang@cqmu.edu.cn (Z. Wang), zhangliang338@cqmu.edu.cn (L. Zhang)

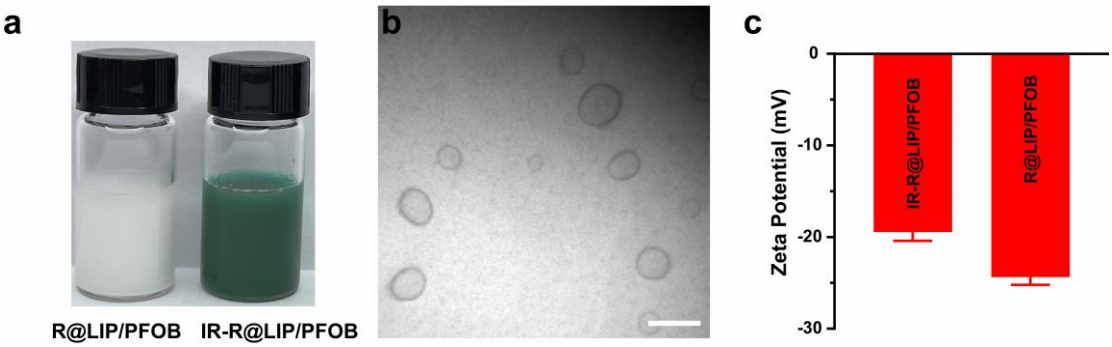

Figure S1 (a) Photographs of R@LIP/PFOB (milky white) and IR-R@LIP/PFOB (dark green) dispersed in PBS. (b) Representative TEM image of IR-R@LIP/PFOB (scale bar = 200 nm). (c) Zeta potential of IR-R@LIP/PFOB and R@LIP/PFOB nanoliposomes.

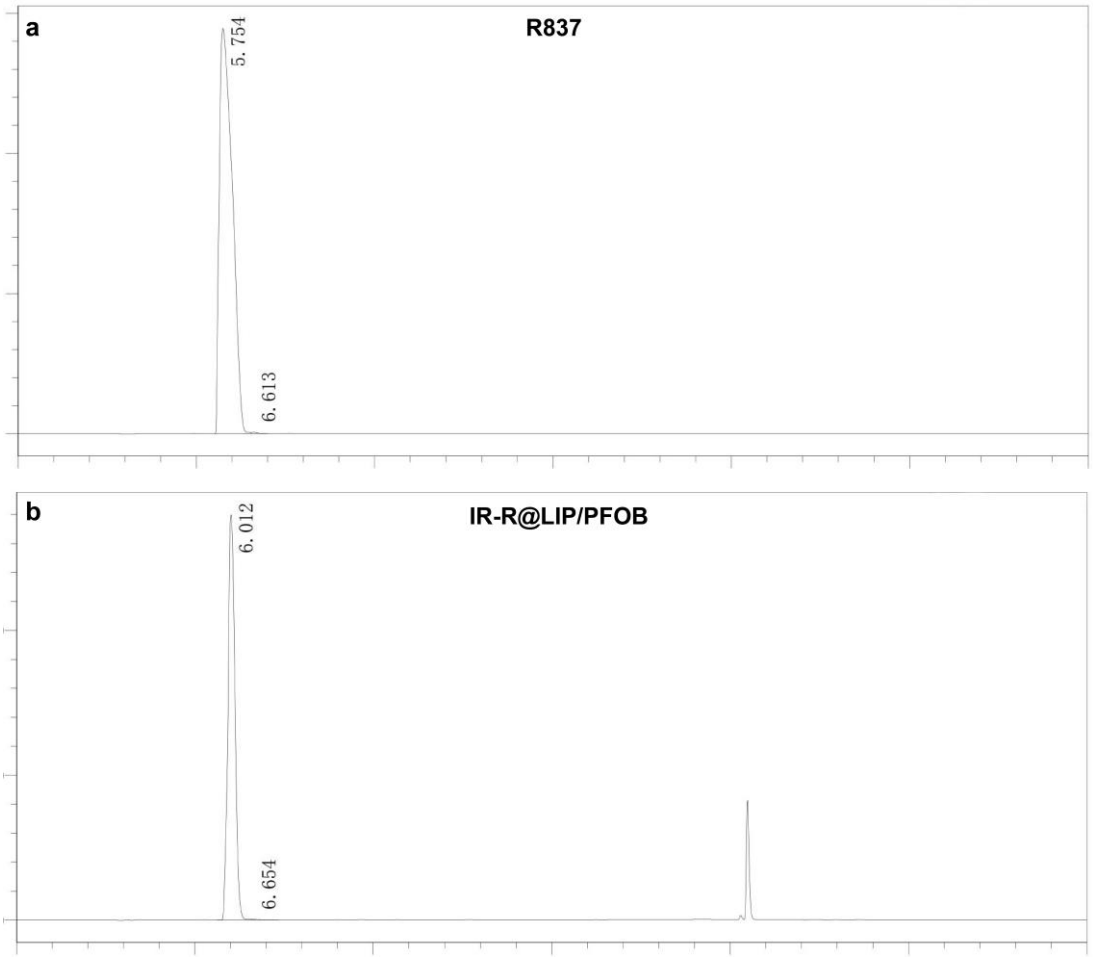

Figure S2 HPLC absorbance of R837 (a) and IR-R@LIP/PFOB (b), indicating the successful encapsulation of R837 into IR-R@LIP/PFOB nanoliposome.

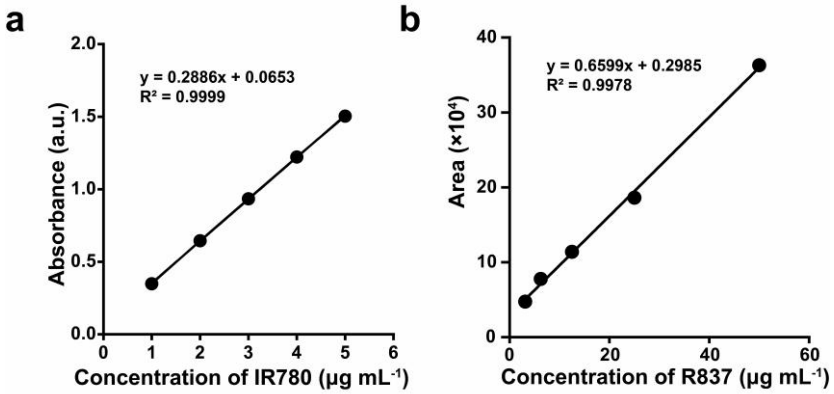

Figure S3 (a) Standard curve of IR780 calculated by UV−vis results. (b) Standard curve of R837 at different concentrations.

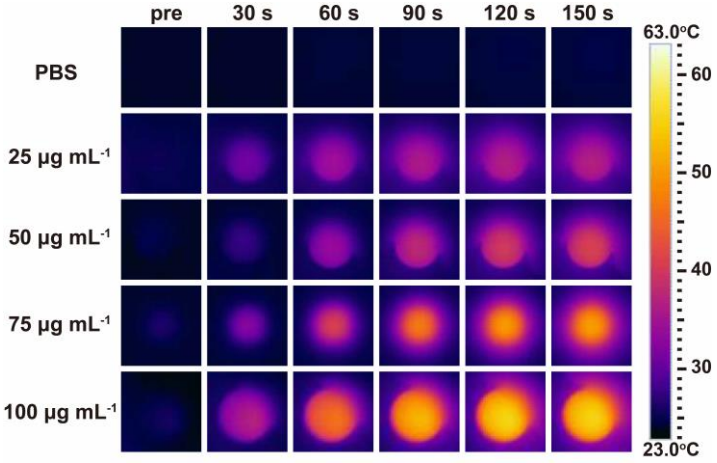

Figure S4 Infrared thermal images of IR-R@LIP/PFOB aqueous solution at different IR780 concentrations under laser irradiation (808 nm, 1.5 W cm^{-2}).

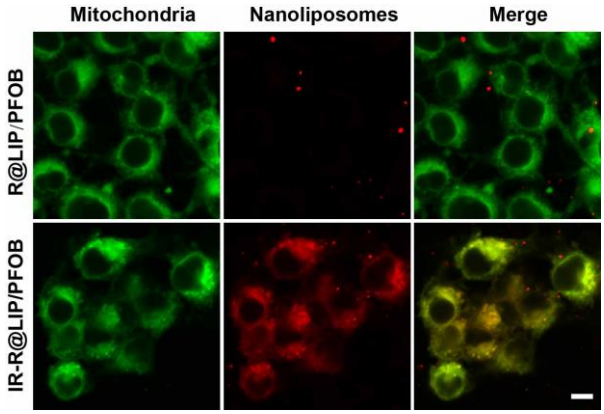

Figure S5 Detailed images for the co-localization of nanoliposomes (DiI-labeled R@LIP/PFOB and IR-R@LIP/PFOB) and mitochondria (scale bar = 10 μm).

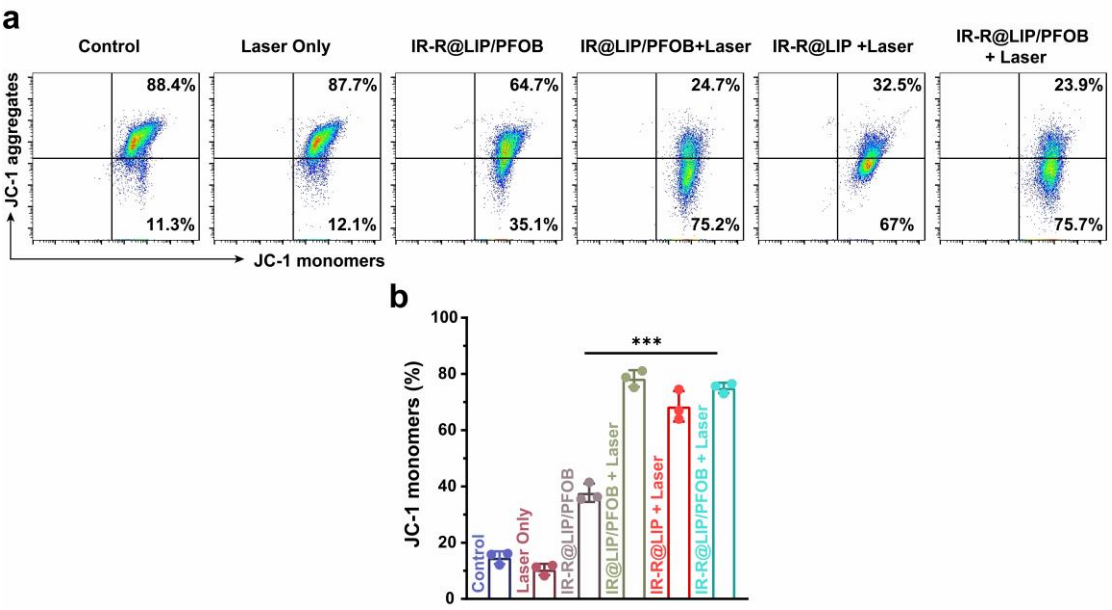

Figure S6 (a) Mitochondria membrane potential of 4T1 cells post different treatments as determined by flow cytometry. (b) Quantitative analysis of JC-1 monomers in 4T1 cells after different treatments as indicated.

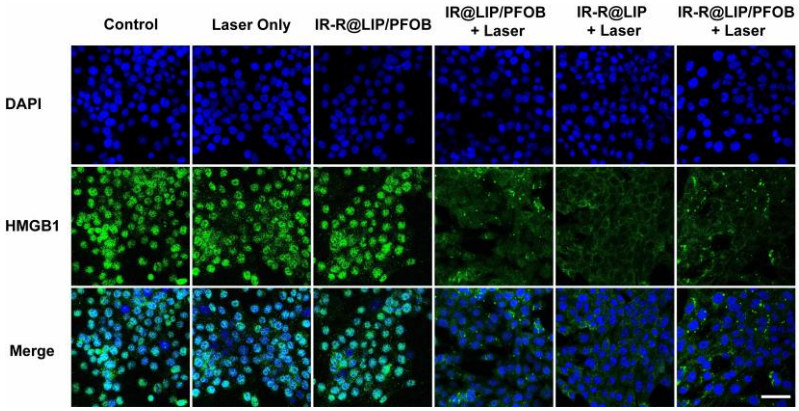

Figure S7 CLSM images illustrating HMGB1 release from 4T1 cells after various treatments (scale bars = 50 μm).

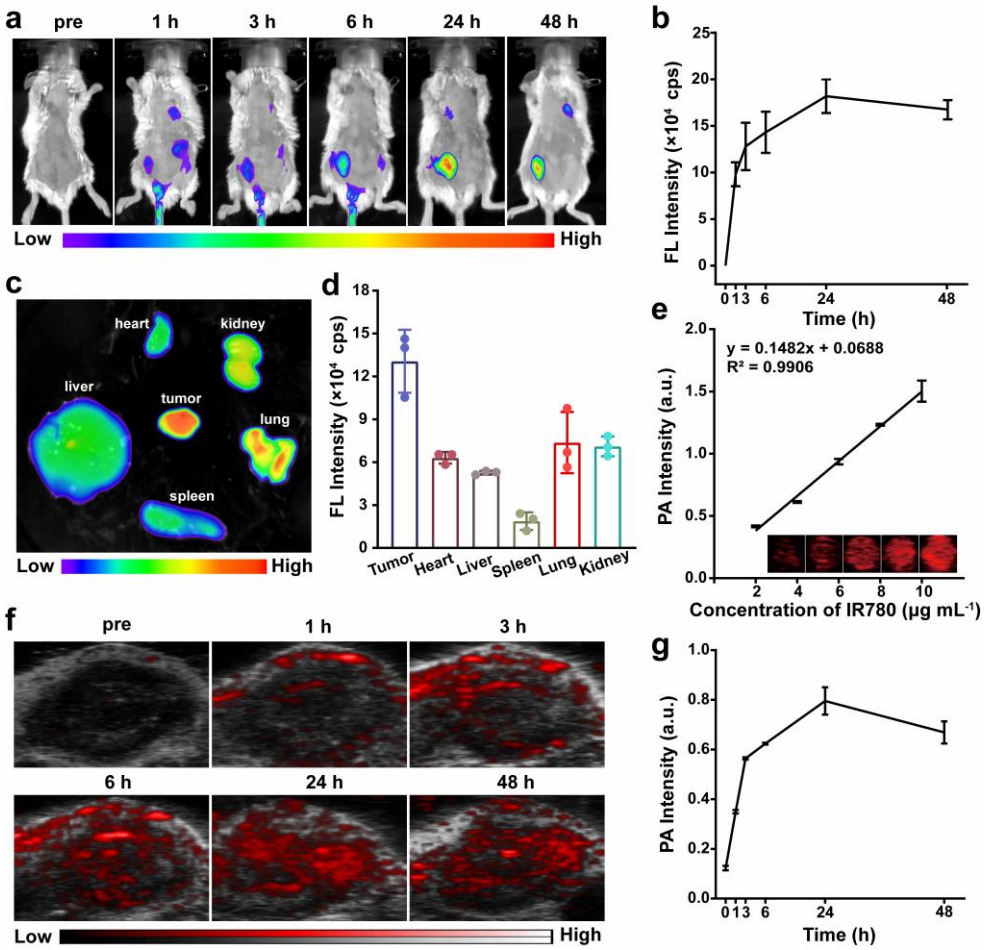

Figure S8 Biodistribution of IR-R@LIP/PFOB. (a-b) FL images and corresponding FL intensities analysis of tumor sites in 4T1 tumor-bearing mice after intravenous injection of IR-R@LIP/PFOB at different time points (n = 3). (c) *Ex vivo* fluorescence images of tumor tissue and major organs (heart, liver, spleen, lung, and kidney) and (d) corresponding FL intensities (n = 3). (e) *In vitro* PA images and PA intensities of IR-R@LIP/PFOB at different IR780 concentrations (n = 3). (f) PA images of 4T1 tumors after intravenous injection with IR-R@LIP/PFOB and (g) corresponding quantitative analysis of PA intensities within tumor sites (n = 3).

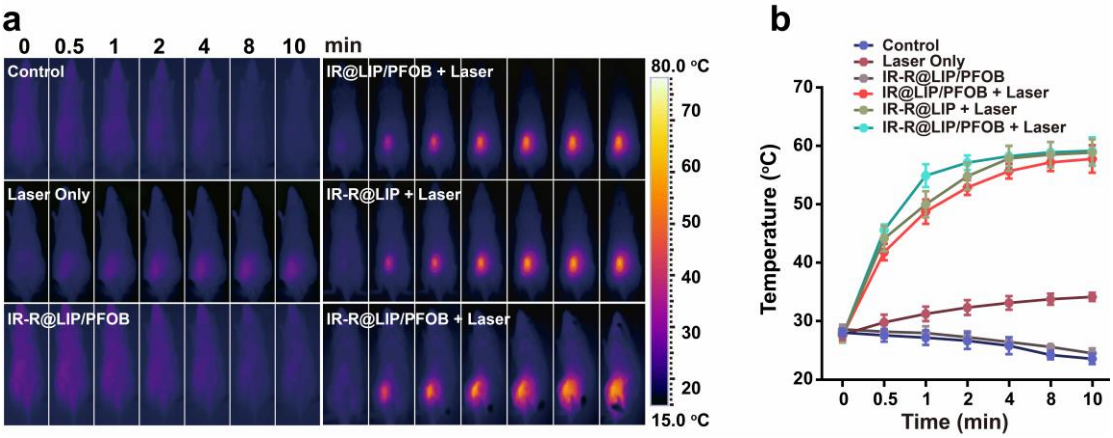

Figure S9 (a) Infrared thermal images of 4T1 tumor-bearing mice in different groups. (b) Photothermal temperature-time curves of tumors in different groups.

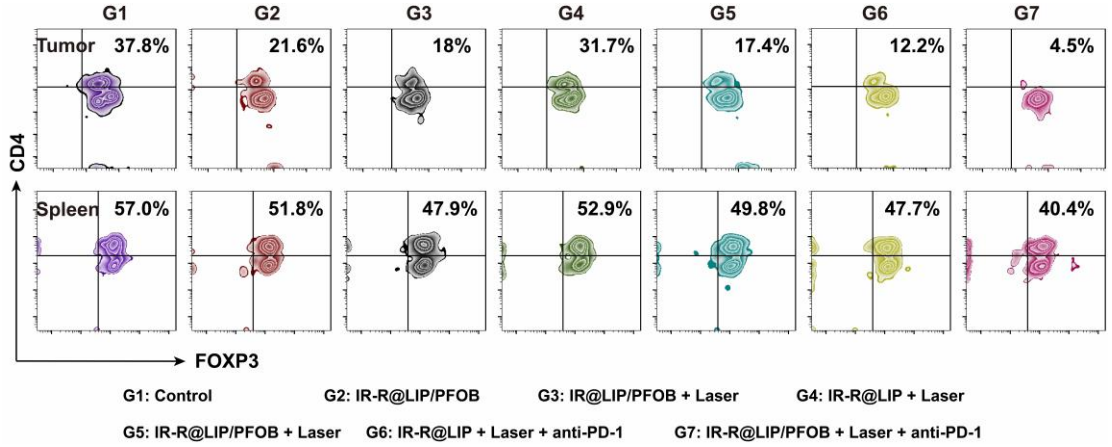

Figure S10 Flow cytometry results of Treg (gated on $Foxp3^+$) in $CD3^+CD4^+$ cells in tumors and spleen after various treatments.

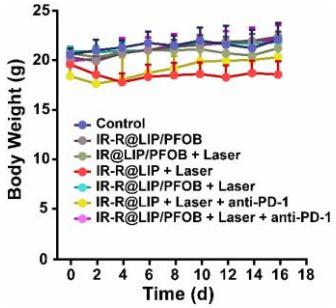

Figure S11 Body-weight changes of mice in different groups.

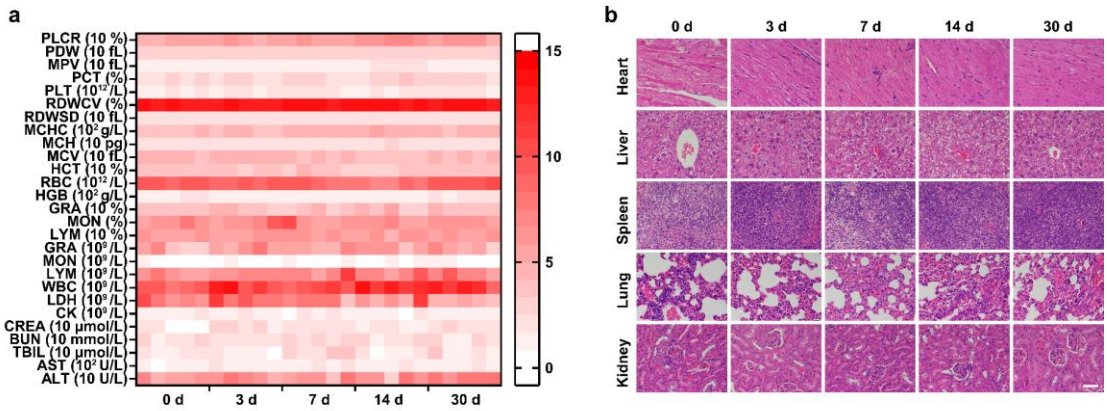

Figure S12 (a) Hematological and blood biochemical test of mice after intravenous administration of IR-R@LIP/PFOB at different time points (0, 3, 7, 14, and 30 d) (n = 5). (b) H&E staining of major organs of mice after varied treatments.